DOI: 10.26599/FSHW.2026.9251361



Contents lists available at CNKI

Food Science and Human Wellness

journal homepage: https://www.sciopen.com/journal/2097-0765

# Polysaccharides from *Hericium erinaceus* mitigate diet-induced obesity by modulating hepatic AMPK signaling and restoring intestinal barrier function via gut microbiota remodeling

Jiacheng Ye[1], Mei Ye[1], Xue Zhou[1], Baoming Tian [1, 2] *

[1.] *College of Food Science and Technology, Zhejiang University of Technology, Huzhou 313299, China*

[2.] *Shaoxing Research Institute, Zhejiang University of Technology, Shaoxing 312000, China*

**ABSTRACT:** Obesity pathogenesis involves a multifaceted interplay between systemic metabolic dysregulation and intestinal microbiota dysbiosis. Using a high-fat diet (HFD)-induced obese mouse model, this research aimed to elucidate the anti-obesity effects and metabolic regulatory functions of *Hericium erinaceus* polysaccharides (HEP). HEP markedly attenuated weight gain and intrahepatic fat deposition, while enhancing systemic glucose disposal and insulin sensitivity. These metabolic improvements were closely associated with modulation of the hepatic AMPK/SREBP-1c signaling pathway, which downregulated lipogenic genes (FAS, ACC, and SREBP-1c) and enhanced lipid catabolism. The reduced metabolic stress subsequently promoted the organization of epithelial intercellular junctions, as demonstrated by the up-regulation of key barrier proteins, including Occludin, Claudin-1, and ZO-1 and the suppression of TLR4/NF-κB-mediated inflammatory cascades. Notably, HEP treatment remodeled the intestinal microbial landscape by fostering the enrichment of advantageous genera (e.g., *Ileibacterium*) and suppressing obesity-related bacteria (e.g., *Lachnoclostridium*). These findings suggested that HEP alleviated obesity by orchestrating a "metabolism-inflammation-microbiota" signaling axis, thereby positioning it as a feasible dietary intervention for the prevention and treatment of obesity.

**Keywords**: *Hericium erinaceus* polysaccharides; obesity; glucose-lipid metabolism; AMPK; gut microbiota; intestinal barrier

## 1. Introduction

Obesity is a chronic and multifactorial metabolic disease typified by abnormal adiposity and high relapse rates following conventional treatments. The shift toward modern dietary patterns is a primary driver of its increasing prevalence [1]. Epidemiological studies indicate a positive correlation between obesity and high-fat diets (HFD). Obesity induced by HFD further contributes to systemic inflammation [2], insulin resistance, diabetes [3] and cancer [4]. HFD-induced obesity is a multifaceted metabolic syndrome fundamentally driven by dysregulated glucose and lipid metabolism. Excessive lipid intake leads to systemic lipotoxicity, as non-adipose tissues fail to fully oxidize surplus fats. This results in ectopic lipid accumulation and stimulates hypertrophic adipocytes to secrete pro-inflammatory cytokines [5, 6]. These inflammatory mediators exacerbate

***Corresponding author**
tbm2020@zjut.edu.cn

Received 3 April 2026
Received in revised from 24 June 2026
Accepted 5 August 2026

insulin resistance, further disrupting glucose homeostasis [7]. Emerging evidence indicates that gut microbiota is not merely associated with obesity but actively participates in its progression through the "metabolism-inflammation-microbiota" axis [8-10]. HFD-induced dysbiosis reduces the production of beneficial microbial metabolites, particularly short-chain fatty acids (SCFAs), leading to the downregulated expression of tight junction proteins and increased intestinal permeability [11]. Consequently, bacterial endotoxins such as lipopolysaccharide (LPS) can translocate into the circulation and activate TLR4/NF-κB-mediated inflammatory signaling, thereby aggravating chronic low-grade inflammation, insulin resistance, and hepatic lipid accumulation [12-14]. Given that conventional interventions, including pharmacotherapy and bariatric surgery, often exhibit limited efficacy or adverse side effects [15-17], simultaneous regulation of gut microbiota composition and intestinal barrier integrity has emerged as a promising therapeutic strategy for obesity.

Increasing evidence indicates that dietary polysaccharides exert anti-obesity activities primarily through prebiotic effects rather than direct absorption. As fermentable macromolecules, polysaccharides selectively promote beneficial bacteria, increase SCFA production, reinforce intestinal barrier integrity, suppress metabolic endotoxemia, and consequently improve systemic metabolic homeostasis [18-20]. Previous studies have demonstrated that HEP exhibits diverse biological activities, including alleviating gut barrier injury [21], improving glucose metabolism and modulating gut microbiota composition [22]. Nevertheless, these investigations have mainly focused on individual physiological outcomes or isolated signaling pathways. Whether HEP simultaneously remodels gut microbiota, restores intestinal barrier integrity, suppresses gut-derived inflammatory signaling, and subsequently regulates hepatic lipid metabolism through the "metabolism–inflammation–microbiota" axis remains inadequately understood. Therefore, unlike previous studies that primarily investigated the anti-inflammatory or hypolipidemic effects of HEP independently, the present study systematically elucidates the integrated regulatory network linking gut microbiota remodeling, intestinal barrier restoration, TLR4/NF-κB inhibition, and hepatic AMPK activation in HFD-induced obesity.

Given the structural potential of polysaccharides and the established "metabolism-inflammation-microbiota" axis, we hypothesize that HEP mitigates obesity through a dual-action mechanism involving the potential modulation of hepatic AMPK/SREBP-1c signaling to suppress lipogenesis, coupled with the indirect modulation of systemic inflammation via the reinforcement of epithelial junctional integrity and the reshaping of gut microbiota. Testing this hypothesis will not only clarify the multi-dimensional regulatory role of HEP in metabolic health but also establish a robust mechanistic foundation for utilizing fungal polysaccharides as targeted functional food interventions for obesity.

## 2. Materials and Methods

### *2.1 Reagents and Experimental Materials*

Insulin was purchased from Biyuntian Biotechnology Co., Ltd (Shanghai, China). The quantitative PCR kit, reverse transcription kit, total RNA extraction kit, phosphatase inhibitors, and PMSF were supplied by Vinocell Biotechnology Co., Ltd (Nanjing, China). One-step PAGE color gel was obtained from Wuhan

Savier Biotechnology Co., Ltd. Protein-free rapid blocking solution and Color Prestained Protein Marker were purchased from Wuhan BOD Biotech Co., Ltd (Wuhan, China). Kits for interleukin-1β (IL-1β), interleukin-6 (IL-6), tumor necrosis factor (TNF-α), leptin (LEP), and insulin (INS) were purchased from Enzyme-Linked Biological Technology Co., Ltd (Shanghai, China). Ultra-sensitive ECL chemiluminescence kit was obtained from Xinsaimei Biotechnology Co., Ltd (Suzhou, China). Levels of total cholesterol (T-CHO), high-density lipoprotein cholesterol (HDL-C), triglycerides (TG), and low-density lipoprotein cholesterol (LDL-C) were measured using kits from Nanjing Jiancheng Biological Engineering Institute (Nanjing, China).

### *2.2 The Methods of Experiment*

#### *2.2.1 Preparation of HEP*

HEP was isolated and purified in accordance with the methodology we detailed in an earlier report [21]. The *Hericium erinaceus* fruiting bodies were dried at 50 °C for 10 h and then pulverized. To remove lipids and pigments, the powder was pre-treated with 95% (v/v) ethanol overnight. After centrifugation, the supernatant was decanted, and the residue was air-dried to eliminate residual ethanol. The defatted powder (100 g) underwent extraction in deionized water at 95 °C for 3 h. This hot water extraction process was performed twice. The combined fractions were centrifuged, and the collected supernatant was evaporated to a smaller volume (42 °C, under vacuum). To precipitate the polysaccharides, the concentrate was brought to 50% (v/v) ethanol by adding food-grade 95% ethanol. After centrifugation, the resulting precipitate was collected and redissolved in purified water. Proteins were eliminated via the Sevag method. The aqueous phase was dialyzed for 72 h through a molecular weight cut-off (MWCO) membrane (3,000 Da) to remove salts and small molecules. After concentration, the solution was lyophilized to obtain crude HEP fraction (precipitated at 50% ethanol). The freeze-dried HEP were stored in a desiccator for subsequent experiments.

According to our previous investigations [23], the chemical composition of HEP was characterized by a total carbohydrate content of 65.01% ± 1.50%, with uronic acids and reducing sugars accounting for 2.40% ± 0.30% and 0.67% ± 0.08%, respectively. HEP is a heteropolysaccharide primarily composed of glucose and galactose, supplemented by fructose and mannose (molar ratio 10.6:10.4:1.7:0.5). Its molecular weight distribution (Mw) features a predominant fraction at 16.72 ± 2.11 kDa (71.68%) alongside a visible shoulder peak. FT-IR analysis further confirmed the polysaccharide nature of HEP, evidenced by characteristic absorption bands for C–H (2900 $cm^{-1}$) and O–H (3400 $cm^{-1}$)–which indicated the presence of hydrogen bonds within or between HEP molecules, reflecting one of the most typical characteristics of polysaccharide substances as well as carboxylate groups (1653 and 1400 $cm^{-1}$). Furthermore, the fingerprint region (1200–1000 $cm^{-1}$) signified a pyranose ring configuration. Morphologically, SEM observations revealed a smooth, sheet-like, and layered surface with minor wrinkles, which demonstrated the typical physical state of the polymer polysaccharides after extraction, concentration and freeze-drying. Structurally, Cui et al. [24] conducted methylation analysis on HEP, and the results elucidated that HEP possessed a backbone of (1→6)-β-D-glucopyranosyl residues (49.32%), branched at the O-3 position with side chains consisting of (1→3)-linked and terminal glucose units.

*2.2.2 Experimental Animals*

The animals were male C57BL/6J mice, which were supplied by the Zhejiang Academy of Medical Sciences (SPF-grade, 8 weeks old, 22–24 g). The animal production license number was SCXK (Zhe)2024-0002. The mice were housed in a SPF barrier facility under controlled conditions: relative humidity of 70% ± 5%, constant temperature of 25 ± 2°C, and a 12-hour light-dark cycle.

Ethical clearance for all experimental work was obtained from the Animal Ethics Committee of Zhejiang University of Technology (No. MGS20241022141). In accordance with ethical standards, experimental procedures were aligned with the ARRIVE guidelines. We strictly observed the statutory requirements of the Animals (Scientific Procedures) Act 1986, the EU Directive 2010/63/EU for scientific animal protection, and the guidelines set by the National Research Council for laboratory animal care.

*2.2.3 Mouse Experiment Design*

Mice were acclimatized for 7 days. Animal experimental design followed the methodology of Tian et al. [25]; mouse gavage dosing referenced the approach of Yoo et al. [26] and our previous research [21, 27]. A total of 30 mice were randomly distributed into three experimental groups (n = 10 per group), as delineated in Table S1. Mice were divided into three groups: low-fat control group (NC), high-fat model group (MC), and high-fat diet + HEP group (HEP, 200 mg/kg). According to the body surface area normalization method recommended by the U.S. Food and Drug Administration (Km: mouse = 3, human = 37), the mouse dose of 200 mg/kg corresponds to a human equivalent dose (HED) of approximately 16.2 mg/kg body weight per day (equivalent to approximately 1.13 g/day for a 70-kg adult) [13, 28]. The selection of the 200 mg/kg dosage was based on preliminary studies and previous literature demonstrating its optimal efficacy in exerting anti-inflammatory and barrier-protective properties without exhibiting observable toxicity in murine models. While this dose is pharmacologically feasible, its translation to human dietary intake requires further assessment, as HED does not equate to typical nutritional consumption levels [24, 29].

The NC and MC groups received double-distilled water via gavage to control for procedural stress. Except for the NC group fed 10% low-fat diet, all other groups received 60% high-fat diet. Specific diets (TPP23302 for 10% low-fat and TP23300 for 60% high-fat) were sourced from TROPHIC Animal Feed High-tech Co., Ltd. (Nantong, China). The comprehensive nutritional profiles of these diets are documented in Table S2.

Animals were fasted for 12 h after 12 weeks of feeding. Following anesthesia, blood samples were collected via retro-orbital venous plexus puncture, and serum was isolated by centrifugation. Concurrently, liver, colon, epididymal fat, and subcutaneous fat were harvested. All tissue samples were kept at −80 °C until needed for downstream processing.

*2.2.4 Oral Glucose Tolerance Test (OGTT) and Insulin Tolerance Test (ITT)*

The ITT and OGTT were conducted following the procedure described by Tian et al. [25] at weeks 11 and 12 of modeling, respectively.

*2.2.5 Mouse Body Weight, Food Intake*

Weight change curves were plotted using the mice's weights recorded every Friday, while daily food intake was also recorded and calculated.

*2.2.6 Histopathological Observation and Analysis*

Following euthanasia, the liver, epididymal fat, subcutaneous fat, and colon tissues were collected. The liver and colon were fixed in 4% paraformaldehyde, and the epididymal fat was fixed in a specialized fat fixative. These tissues were embedded and sectioned into 4 μm thick sections. For histological evaluation, hematoxylin and eosin (H&E) staining was performed on the collected tissue sections.

Organ index = organ weight / mouse weight.

*2.2.7 Determination of Serum Biochemical Parameters*

Blood samples were centrifuged to isolate serum for subsequent analyses. Serum lipid profiles, including T-CHO, LDL-C, HDL-C, and TG were determined via specific commercial kits. In addition, the levels of pro-inflammatory cytokines, LEP and INS were measured using ELISA kits.

*2.2.8 mRNA Expression Levels in Mouse Tissues*

RT-qPCR was employed to evaluate mRNA expression in murine tissues, following RNA extraction via the TRIzol method and concentration measurement using a micro-volume analyzer. cDNA reverse transcription and quantitative amplification were performed. Relative transcript abundance was evaluated based on the $2^{-\triangle\triangle Ct}$ method. The primer sequences used in this study are listed in Table S3.

*2.2.9 Western Blot Analysis*

Liver and colon tissues were homogenized in RIPA lysis buffer supplemented with phosphatase and protease inhibitors. Total protein concentration was subsequently determined. After transferring the SDS-PAGE-resolved proteins to a PVDF membrane and blocking at room temperature, primary antibody binding was allowed to proceed at 4 °C overnight (12–16 h). Afterward, the membrane was treated with a matching secondary antibody for 60 min. Signals were detected using Western Lighting Plus ECL chemiluminescent substrate. Optical density was quantified using ImageJ version 1.41.6.

*2.2.10 16S rDNA High-Throughput Sequencing for Intestinal Microbiota Analysis*

Fresh fecal samples were collected prior to euthanasia for genomic DNA extraction. Following total DNA extraction from samples, primers 338F (5'-ACTCCTACGGGAGGCAGCA-3') and 806R (5'-GGACTACHVGGGTWTCTAAT-3') were utilized. PCR amplification was performed, followed by purification, quantification, and normalization to form sequencing libraries. After quality assessment, the Illumina NovaSeq 6000 platform was utilized to sequence the libraries, and the resulting data were processed through the BMKCloud online analysis platform (https://www.biocloud.net).

*2.2.11 Analysis of Short-Chain Fatty Acids*

Samples were centrifuged to collect the supernatant (500 μL), which was subsequently combined with 100 μL of crotonic acid-metaphosphoric acid solution. Following thorough vortexing, the preparation was acidified and kept at -80 °C for 24 h prior to further analysis. After acidification, samples were thawed at 4°C and centrifuged at 10,000 rpm, and the clarified solution was filtered through a 0.22 μm membrane. SCFA concentrations were determined via gas chromatography analysis. Detection was implemented using a DB-FFAP column with crotonic acid as the internal marker. The injection port temperature was set at 250 °C. The gas chromatography (GC) analysis employed an initial oven temperature of 75 °C, with a two-stage ramp: first to 180 °C (20 °C/min, 1 min hold) and then to a final 220 °C (40 °C/min, 1 min hold). The flame ionization detector (FID) was operated at 250 °C, and a 1-μL sample was injected for each run.

*2.2.12 Data Analysis and Processing*

Data processing was performed with IBM SPSS Statistics 26 (Armonk, NY, USA). Intergroup comparisons were performed using one-way ANOVA followed by Tukey's post hoc test. All values are reported as mean ± SEM with the number of replicates indicated. Statistical significance: $*P < 0.05$ and $**P < 0.01$ versus the NC group; $\#P < 0.05$ and $\#\#P < 0.01$ versus the MC group.

## 3. Results

*3.1 Analysis of Weight Gain and Food Intake in High-Fat Diet-Induced Mice Using HEP*

The establishment of the HFD mouse model is shown in Figure 1. A schematic representation of the animal experimental procedure is provided in Figure 1A. As expected, HFD feeding significantly accelerated mouse weight gain (Figures 1B and 1C). Compared to NC group, the MC group exhibited a 38.1% increase in body weight ($P < 0.01$). However, HEP administration significantly attenuated this excessive weight gain ($P < 0.05$). As illustrated in Figure 1D, although the MC group exhibited slightly lower food consumption than the NC group, this difference was not statistically significant ($P > 0.05$). Furthermore, supplementation with HEP did not significantly alter the daily food intake. In summary, HEP intake suppressed excessive weight gain without significantly affecting food intake in mice.

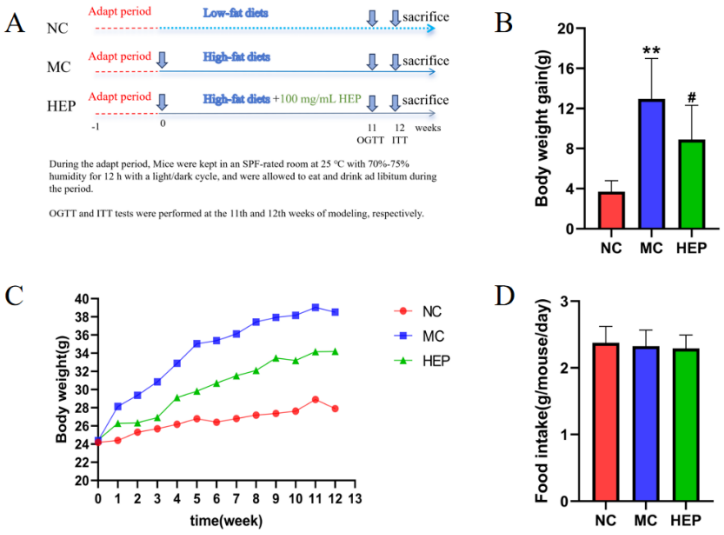



**Figure 1.** Impact of HEP on body weight and food intake in HFD-induced mice (A) Schematic diagram of animal experiment; (B) Mouse weight gain; (C) Mouse weight change; (D) Mouse food intake

### *3.2 Effects of HEP on ITT and OGTT in High-Fat Diet-Induced Mice*

Figure 2A and 2B illustrate the results of the ITT in mice. HFD consumption triggered a substantial increase in the ITT area under the curve (AUC) relative to the NC group ($P < 0.01$), indicating severe insulin resistance. In contrast, the HEP group exhibited a significant reduction in the ITT AUC relative to the MC group ($P < 0.01$), indicating that HEP intake effectively improved insulin sensitivity in mice, thereby enhancing insulin regulation of glucose homeostasis. As depicted in Figure 2C and 2D, HFD feeding led to a substantial rise in the OGTT AUC relative to the NC group ($P < 0.01$), while a significant reduction was exhibited in the HEP group ($P < 0.01$). Consequently, these findings demonstrate that HEP possesses a potent capacity to restore glycemic homeostasis in HFD-fed mice.

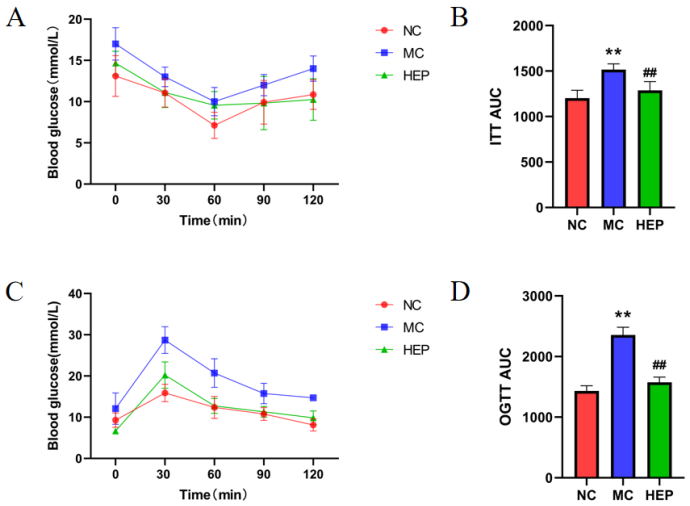



**Figure 2.** Effects of HEP on HFD-induced insulin resistance in mice (A)ITT; (B) AUC of the ITT; (C) OGTT; (D) AUC of the OGTT

### *3.3 Effects of HEP on Mouse Anatomy and Tissue*

Figure 3A displays representative macroscopic images of mice. The MC group exhibited pronounced fat deposition and increased body weight relative to the NC group. By contrast, HEP treatment effectively curbed body weight gain and attenuated adipose tissue expansion. Livers from the MC group appeared hypertrophic and pale compared to those in the NC group (Figure 3B). Conversely, the livers in the HEP group were visibly smaller and exhibited a restored, darker reddish-brown color compared to those in the MC group. Figure 3C shows representative images of epididymal fat pads from the three groups. The epididymal adipose tissue volume substantially increased in the MC group versus the NC group, an effect that was visibly reduced following HEP therapy.

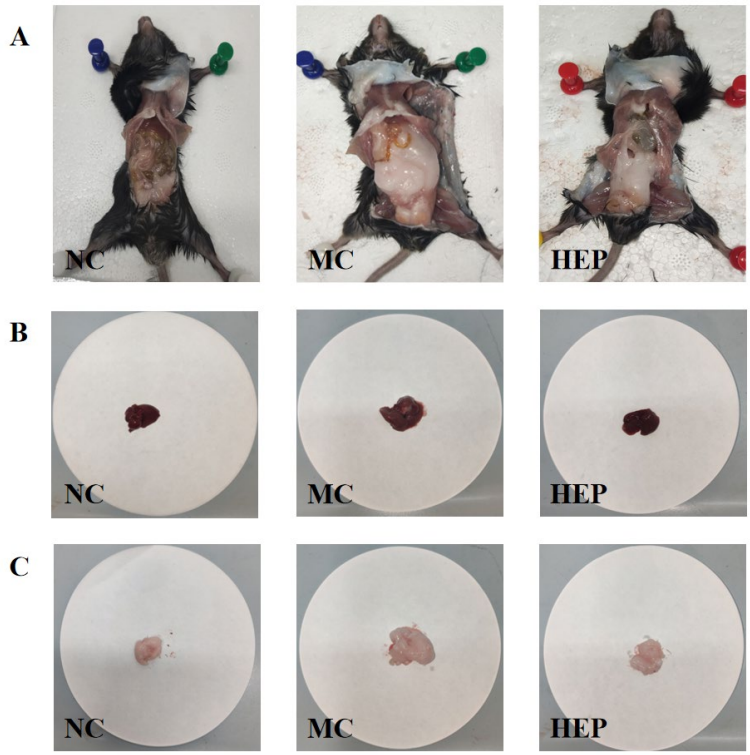



**Figure 3.** Anatomical and tissue comparison among different treatment groups in mice (A) Mouse dissection images; (B) Liver; (C) Epididymal fat

### *3.4 Histological Analysis of Liver Tissue*

Figure 4A shows H&E-stained liver tissues. In the NC group, no obvious lipid vacuoles were observed in the liver. Hepatocyte nuclei were centrally located, sinusoids were clearly defined, and hepatic cords were well-organized. In contrast, hepatocytes in the MC group contained numerous lipid vacuoles of varying sizes, with densely distributed lipid droplets appearing swollen and disorganized. Cell boundaries were indistinct, and inflammatory changes were present, confirming successful establishment of HFD-induced hepatic injury. Compared to the MC group, the HEP group displayed a marked reduction in intracellular lipid vacuoles, with cells exhibiting improved alignment and reduced swelling. Cellular morphology resembled that of the NC group, featuring well-defined sinusoids, regular hepatic cords, and no significant inflammatory infiltration. This demonstrated that HEP alleviated liver damage induced by HFD.

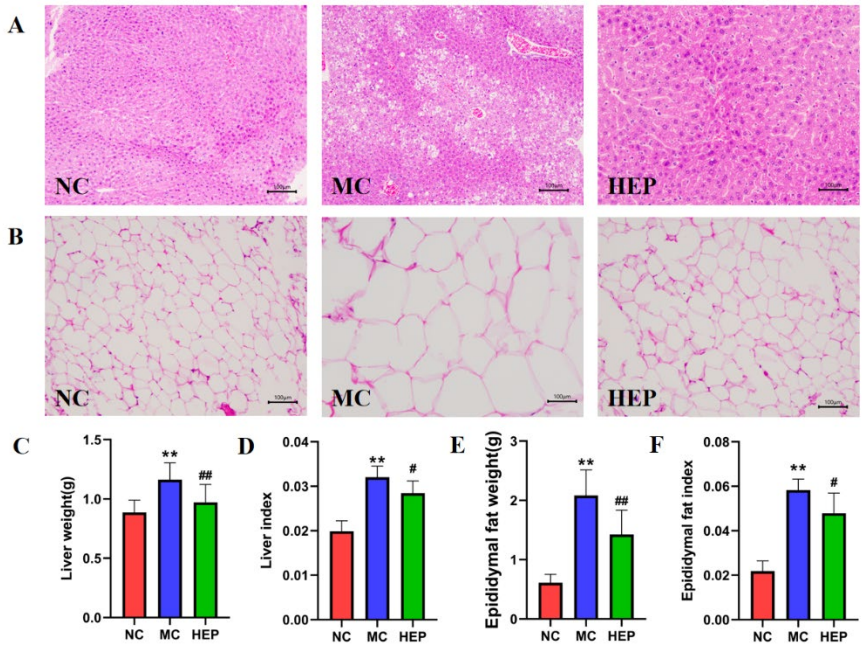



**Figure 4.** Effects of HEP on liver organization and epididymal adipose (A) Liver H&E staining; (B) H&E staining of epididymal adipose tissue; (C) Liver weight; (D) Liver index; (E) Epididymal fat weight; (F) Epididymal fat index

### *3.5 Epididymal Fat Tissue Morphology Analysis*

As depicted in Figure 4B, histological evaluation of H&E-stained epididymal fat revealed that, compared to the NC group, adipocytes in the MC group exhibited severe hypertrophy and narrowed intercellular spaces, indicative of abnormal lipid accumulation. This indicated that mice in the MC group presented typical pathological features of metabolic disorder, whereas the NC and HEP groups maintained normal adipose tissue structure with intercellular spaces returning to uniformity. Both epididymal fat weight and fat index were also significantly increased in the HFD group ($P < 0.01$). After HEP intervention, fat weight in the HEP group reduced notably ($P < 0.01$), and fat index also showed a marked reduction ($P < 0.05$). In summary, the HFD induced pathological hypertrophy of epididymal adipocytes and tissue structural disruption, while HEP intake exerted a protective effect by regulating adipocyte expansion.

### *3.6 Intestinal Tissue Morphology Analysis*

Figure S1 shows the H&E-stained mouse colon tissues. Relative to the NC group, the colonic submucosal layer presented edema, loss of crypt structure, and a significant decline in goblet cell numbers in the MC group. In contrast, the HEP group illustrated significantly alleviated submucosal edema, with restored crypt architecture. Therefore, HEP intervention significantly ameliorates pathological damage in mouse colonic tissue, promotes cellular morphology recovery, and mitigates susceptibility to intestinal inflammation.

### *3.7 Effects of HEP on Serum Biochemical Factors*

Relative to the NC group, LDL-C, T-CHO, and TG concentrations were significantly elevated ($P < 0.01$) in the MC group, while HDL-C concentration was markedly decreased ($P < 0.01$) (Figure 5 A-D). Serum LDL-C and TG levels were substantially reduced ($P < 0.01$) after HEP administration, while T-CHO concentration was significantly declined ($P < 0.05$) and HDL-C concentration was substantially elevated ($P < 0.01$). These findings indicated that HEP effectively reduced systemic lipid factor concentrations and exhibits

lipid-lowering effects. As shown in Figures 5E and F, serum INS and LEP levels in the MC group were notably higher than those in the NC group ($P < 0.01$), indicating that HFD induction caused hyperinsulinemia and hyperleptinemia in mice. HEP administration effectively normalized the elevated INS and LEP concentrations seen in the MC group ($P < 0.01$), indicating a restoration of insulin and leptin homeostasis.

Figure 5G-I depicts the regulatory influence of HEP on serum inflammatory markers in HFD-challenged mice. The levels of pro-inflammatory cytokines (IL-6, TNF-α, and IL-1β) were significantly up-regulated in the MC group versus the NC group ($P < 0.01$). However, HEP intervention reversed the HFD-induced inflammatory response by downregulating the serum concentrations of IL-1β ($P < 0.01$), TNF-α ($P < 0.01$), and IL-6 ($P < 0.05$).

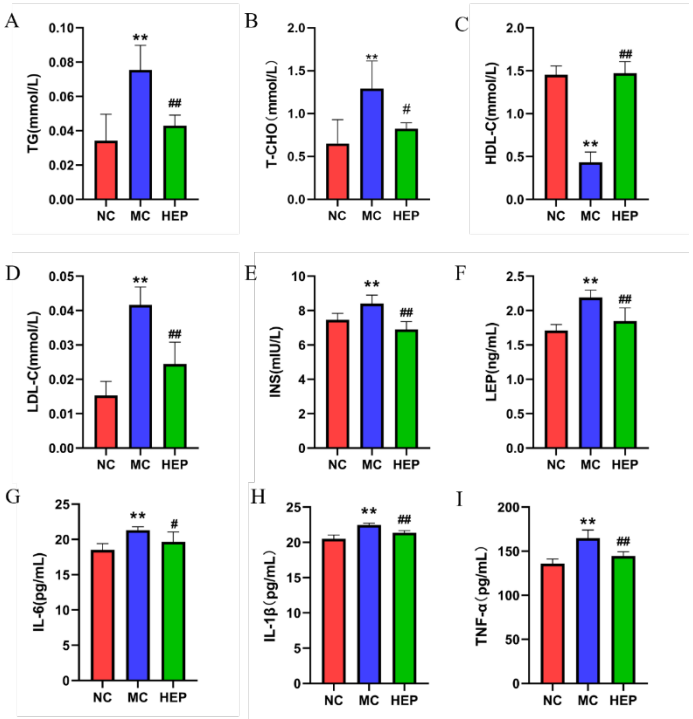



**Figure 5.** Effects of HEP on serum levels of biochemical factors in HFD-induced mice (A) TG; (B) T-CHO; (C) HDL-C; (D) LDL-C; (E) INS; (F) LEP; (G) IL-6;(H) IL-1β; (I) TNF-α

### *3.8 Regulation of HEP on the Levels of Lipid Metabolism mRNA and Proteins in Mouse Liver Tissues*

As shown in Figure 6, after HFD induction, genes involved in lipid metabolism and energy regulation (AMPKα1, PPAR-α, PGC-1α) were significantly downregulated ($P < 0.05$), whereas genes associated with lipid synthesis (SREBP-1C, PPAR-γ, FAS, ACC) were notably upregulated ($P < 0.01$). HEP treatment reversed these alterations. Compared to the NC group, HFD consumption markedly decreased the hepatic p-AMPK/AMPK ratio while significantly increasing the expression of lipid synthesis-related proteins (FAS, ACC, SREBP-1c) ($P < 0.01$). Following HEP intervention, the hepatic p-AMPK/AMPK ratio was significantly increased, and the expression of FAS, ACC, and SREBP-1c was markedly reduced ($P < 0.01$), suggesting that HEP was associated with suppressed lipogenesis and enhanced lipid metabolic regulation. Taken together, these results suggested that modulation of hepatic lipid metabolism may contribute to the lipid-lowering effects associated with HEP treatment.

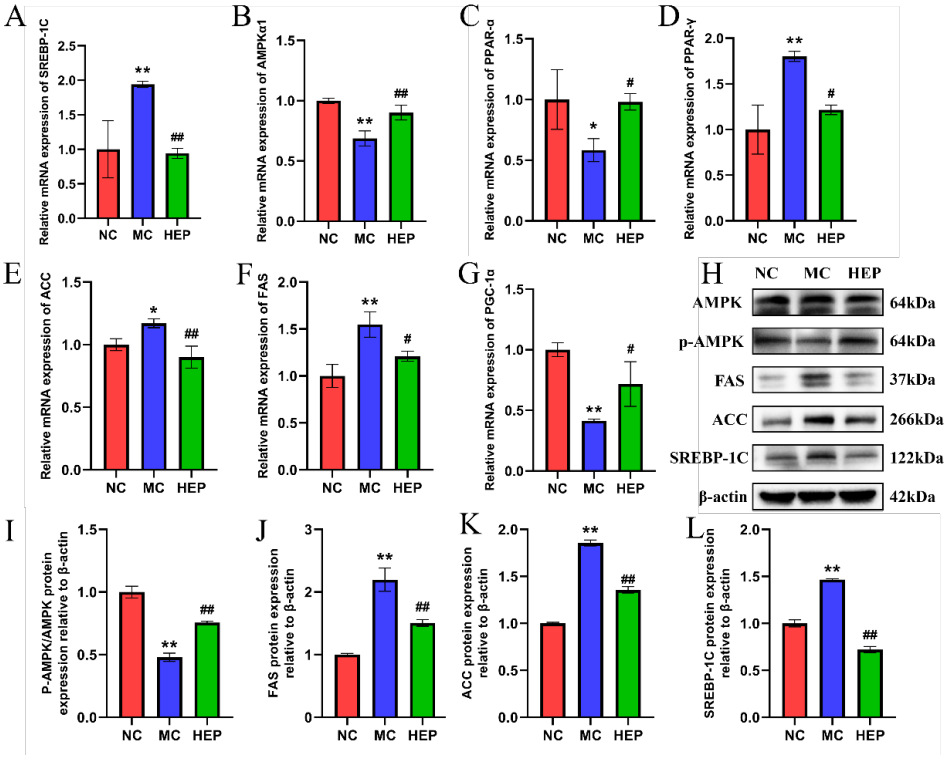



**Figure 6.** Regulation of HEP on the levels of lipid metabolism mRNA and proteins in the mouse liver (A) SREBP-1c; (B) AMPKα1; (C) PPAR-α; (D) PPAR-γ; (E) ACC; (F) FAS; (G) mRNA expression of PGC-1α; (H) Protein expression level associated with lipid metabolism; Relative protein expressions of (I) p-AMPK/AMPK; (J) FAS; (K) ACC; (L) SREBP-1C

### *3.9 Effects of HEP on Inflammation-Related mRNA and Protein Expression in Mouse Colon Tissues*

Figure 7 presents the mRNA and protein expression levels related to intestinal inflammation in mice, demonstrating the regulation of key inflammatory cascades. The mRNA expression levels of inflammation-related genes (TNF-α, TLR4, NF-κB) were substantially elevated in HFD ($P < 0.01$), and this upregulation was reversed after HEP intervention (Figures 7A-C). HEP intervention downregulated TLR4 protein expression (Figure 7E) in HFD-induced mice, reversed the HFD-induced upregulation in IKKα/β level, and downregulated the phosphorylation of NF-κB p65 (Figures 7F and 7G). Compared to the HFD-fed group, HEP-treated mice showed a substantial reduction in TLR4 and p-NF-κB p65 levels ($P < 0.01$), both of which had been prominently increased by the HFD relative to the NC group ($P < 0.01$). Collectively, these results suggested that HEP demonstrated significant suppression of NF-κB pathway activation in response to TLR4 signaling in HFD-induced mice.

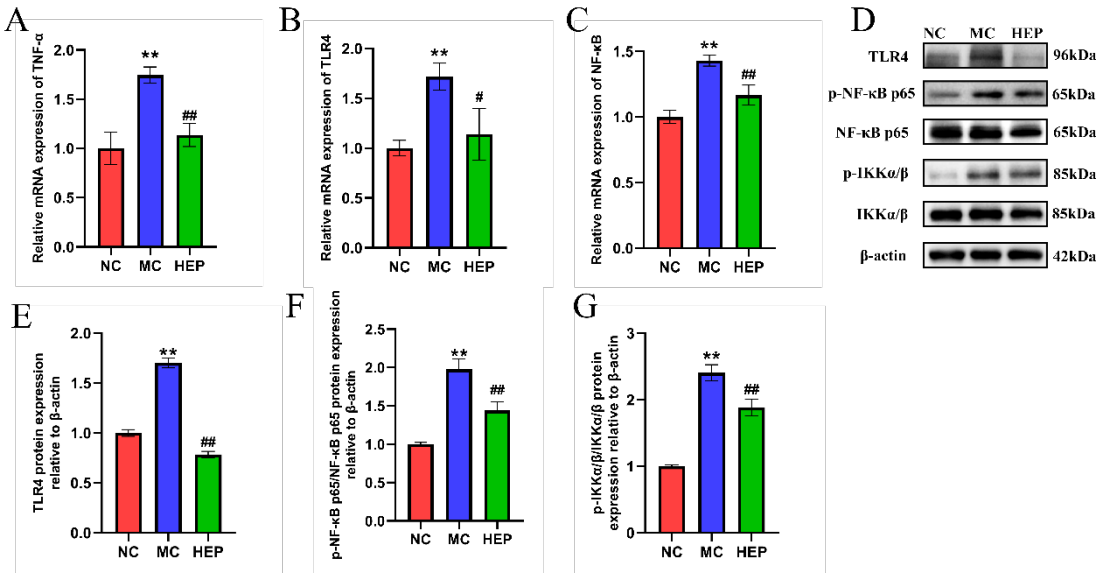



**Figure 7.** Expression of inflammation-related mRNA and proteins in the mouse colon (A) TNF-α; (B) TLR4; (C) mRNA expression of NF-κB; (D) Expression levels of proteins associated with intestinal inflammation; Relative protein expressions of (E) TLR4; (F) p-NF-κB p65/NF-κB p65; (G) p-IKKα/β/IKKα/β

### *3.10 Effects of HEP on the Expression Levels of Tight Junction-Related mRNAs and Proteins in Mouse Colon Tissues*

The intestinal mucosal barrier plays an essential role in preventing direct contact between the intestinal epithelium and harmful agents, including pathogens and endotoxins. The effect of HEP on tight junction integrity in the mouse colon is depicted in Figure 8. Chronic HFD intake led to a substantial reduction in both the mRNA and protein expression levels of intestinal tight junction proteins relative to the NC group ($P < 0.01$), illustrating that HFD impaired intestinal barrier integrity. However, HEP intervention upregulated the levels of these mRNAs significantly ($P < 0.01$). Consistent with the mRNA data, levels of these tight junction protein markers followed a similar pattern. It can be concluded that HEP helps restore intestinal barrier integrity impaired by HFD and may inhibit the translocation of harmful substances, contributing to its anti-obesity effect in mice.

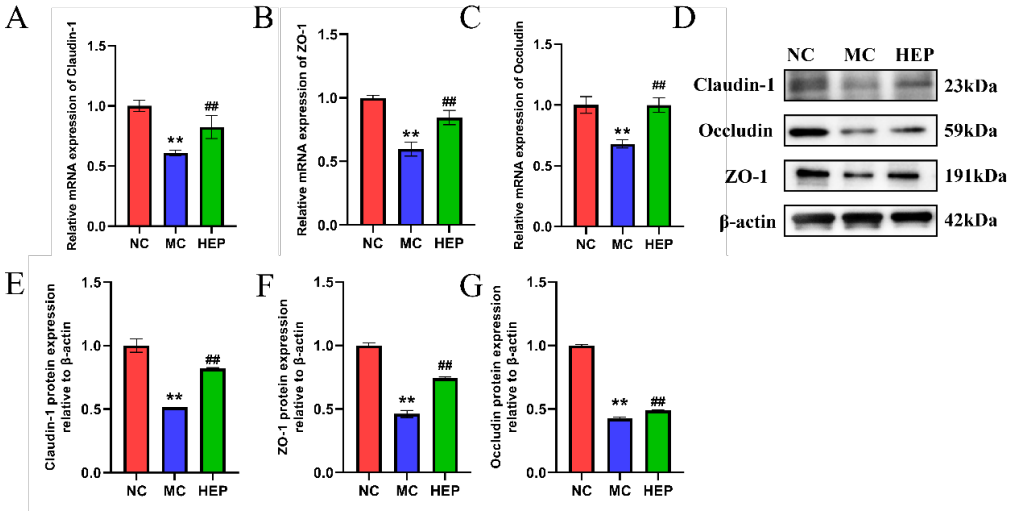



**Figure 8.** HEP on inflammation and tight junction-related mRNA and protein expression in the colon of HFD-induced mice (A) Claudin-1; (B) ZO-1; (C) mRNA expression of Occludin; (D) expression levels of tight junction-related proteins; Relative protein expressions of (E) Claudin-1; (F) ZO-1;(G) Occludin

### *3.11 The Effects of HEP on the Gut Microbiota*

#### *3.11.1 Sequencing Data Quality Assessment*

As indicated by the rarefaction curve in Figure S2A, when the number of sampled sequences was less than 10,000, the number of features increased rapidly with the growth in sampled sequences; When the sampled sequences exceeded 20,000, the growth rate of features slowed down. Beyond 30,000 sampled sequences, the number of features showed no significant further increase. This indicated that the species count of the fecal microbiota did not elevate substantially with higher sequencing depths. Thus, the coverage employed was adequate to reflect the diversity of fecal microbial species. The sequencing data for the samples was comprehensive and reliable. Figure S2B showed that the Shannon index curve leveled off after 5,000 sampled sequences, indicating data saturation. The sequencing depth was sufficient to capture adequate species characteristics, reaching a plateau phase. Figure S2C showed that the rank-abundance curves for each group exhibited discrepancies in both richness and evenness, demonstrating that the sequencing saturation was adequate to cover the majority of species. Figure S2D's species accumulation curve showed that, given the number of samples, the species accumulation curve reached a plateau, meaning that the accumulation of gut microbiota species increased slowly. This demonstrated that the sampling was adequate and the data analysis was reliable.

#### *3.11.2 The Effect of HEP on ASV in the Mouse Intestinal Microbiota*

The effects of HEP on ASVs in the mouse gut microbiota are depicted in Figure S3. Figure S3A and B revealed that a total of 6,364 ASVs were observed. A reduction in ASVs was noted in the HEP group versus the MC group, validating that HEP administration actively reshapes the intestinal microecology. Figure S3C indicated that 255 ASVs were commonly identified across all three groups. The number of group-specific ASVs varied among experimental groups, with the MC group containing 2307, while the NC and HEP groups displayed lower counts of 1994 and 1395, respectively. These analyses collectively demonstrated that HEP exerted a profound regulatory impact on the intestinal flora of mice.

#### *3.11.3 Effects of HEP on α Diversity of Gut Microbiota*

The study employed the Shannon index, PD_whole_tree index, Simpson index, Ace index, and Chao1 index, and cover rate to assess α diversity in the mouse intestinal microbiota. α diversity analysis (Figure 9) revealed decreased ACE and Chao1 indices in the HFD group ($P < 0.05$), while the HEP group showed elevated indices. This indicated that the HFD downregulated richness and diversity of the gut microbiota, and HEP intervention alleviated this effect. The Simpson index and Shannon index in the MC group were notably elevated ($P < 0.01$), while after HEP intervention, the mice showed significant reductions ($P < 0.05$). After HFD intervention, the PD_whole_tree index in the MC group was markedly decreased ($P < 0.01$), further confirming that HFD reduced gut microbiota diversity. Sequencing coverage for all groups approached 1, meeting sequencing requirements. The above data indicated that HEP treatment exerted notable effects on the gut microbiota of HFD-induced mice.

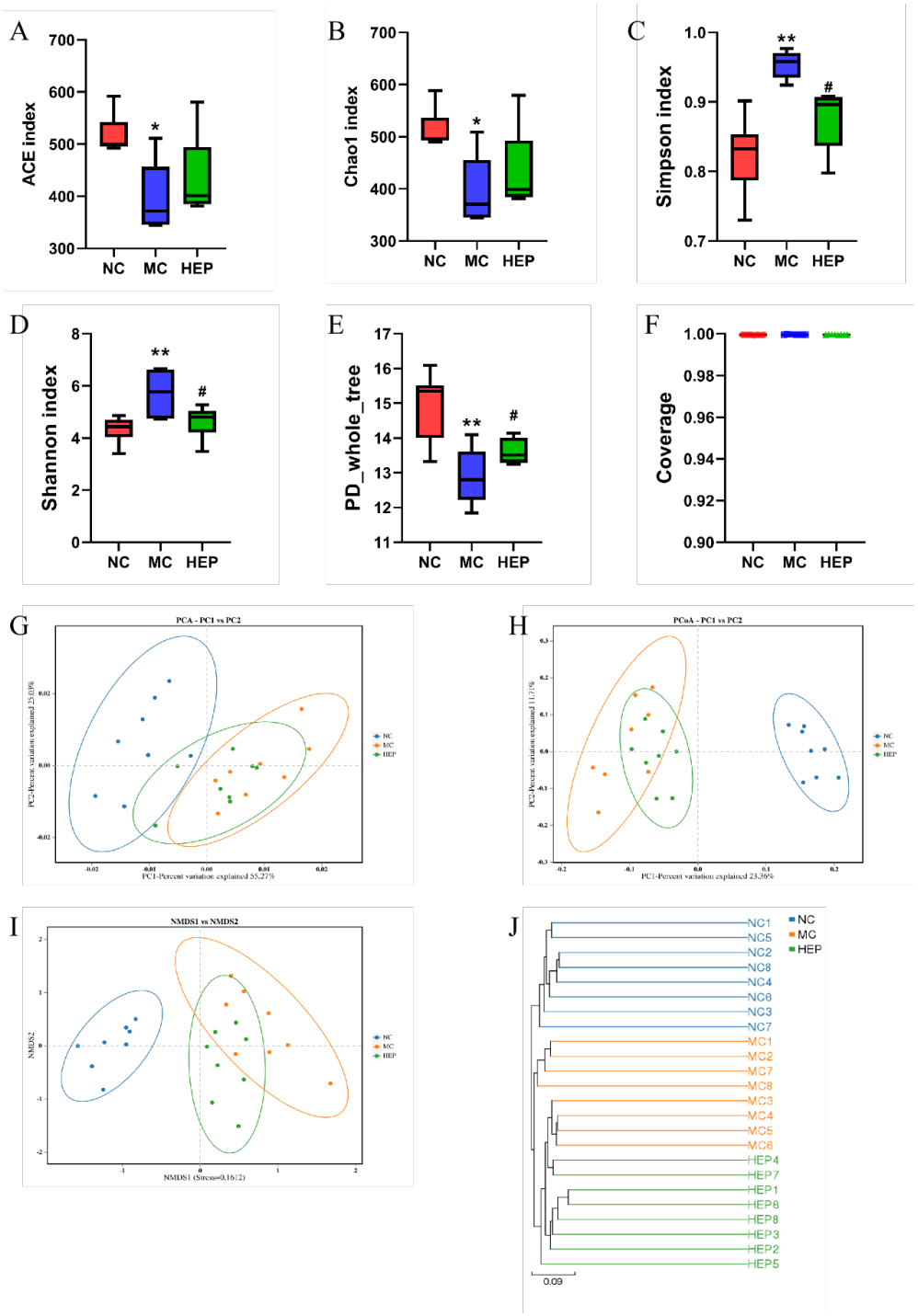



**Figure 9.** α and β diversity analysis (A) ACE index; (B) Chao1 index; (C) Simpson index; (D) Shannon index; (E) PD_whole_tree; (F) Coverage; (G) PCA; (H) PCoA; (I) NMDS; (J) UPGMA

### *3.11.4 Effects of HEP on β-Diversity of the Mouse Gut Microbiota*

As illustrated in Figure 9G, PCA indicated that PC1 and PC2 accounted for 55.27% and 25.03% of the total variance, respectively. The NC group samples clustered on the left side, while the MC group samples were primarily distributed on the right, with the two groups completely separated, indicating successful establishment of HFD-induced gut dysbiosis. Notably, the HEP group showed a distinct shift away from the MC group, clustering intermediately. The PCoA analysis (Figure 9H) demonstrated distinct segregation among the three groups, with the HEP samples positioned markedly closer to the NC group. In the NMDS

analysis (Figure 9I), the stress value of 0.1612 indicated reliable data. Results were consistent with PCA and PCoA findings, confirming that HEP induced changes in the gut microbiota. Figure 9J showed UPGMA analysis, where NC and MC mice formed two distinct branches, while MC and HEP groups exhibited clear differentiation, confirming the role of HEP in altering mouse gut microbiota composition.

### *3.11.5 Effects of HEP on the Phylum Level of the Gut Microbiota*

At the phylum level, Bacteroidota, Firmicutes, Verrucomicrobiota, and Actinobacteriota were the four most abundant phyla. HFD feeding disrupted the microbial profile, evidenced by a sharp increase in the Firmicutes/Bacteroidota (F/B) ratio and the relative abundance of Firmicutes and Actinobacteriota, whereas the proportion of Verrucomicrobiota was significantly diminished compared to the NC group ($P < 0.01$). HEP intervention significantly reduced the abundance of Firmicutes, Actinobacteriota and the F/B ratio ($P < 0.05$), while markedly increasing the relative abundance of Verrucomicrobiota. These findings indicated that HEP altered the microbial structure in HFD-induced mice at the phylum level.

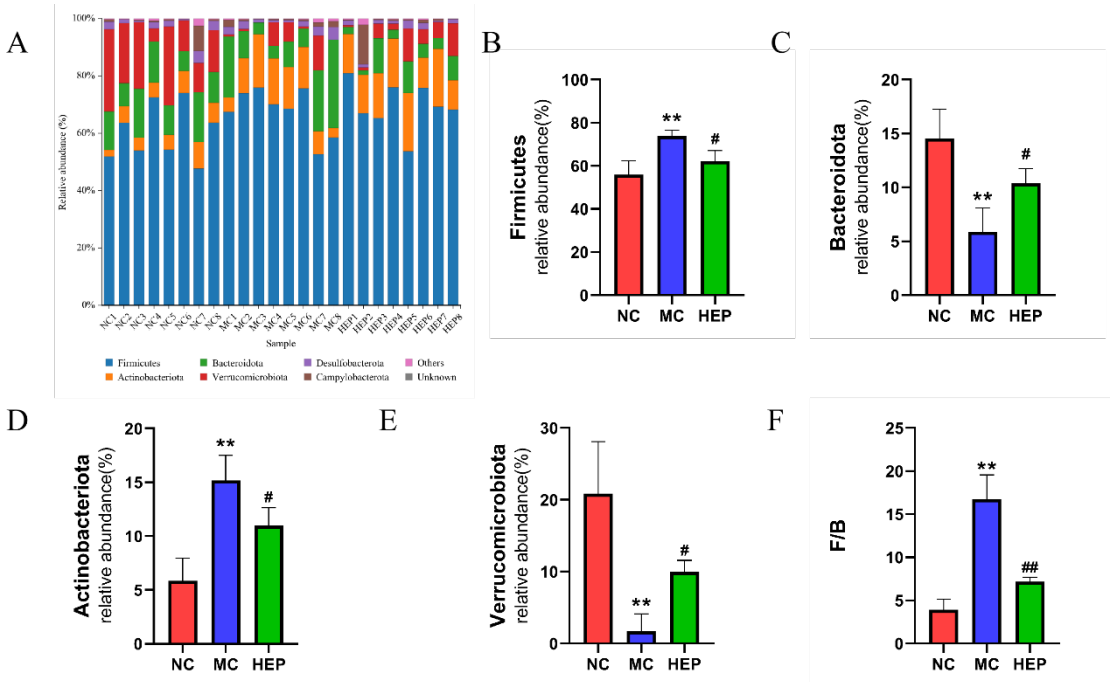



**Figure 10.** Phylum-level Microbiome Analysis (A) Phylum-level microbiome distribution; (B) Firmicutes; (C) Bacteroidota; (D) Actinobacteriota; (E) Verrucomicrobiota; (F) F/B ratio

### *3.11.6 Effects of HEP on the Gut Microbiota of Mice at the Genus Level*

As depicted in Figure 11, the composition of bacterial taxa with relative abundance greater than 1% was analyzed. Relative to the NC group, the abundances of *Lachnoclostridium*, *unclassified_Lachnospiraceae*, *Faecalibaculum*, *Romboutsia*, and *Blautia* were markedly enriched in the MC group ($P < 0.01$), while *Bacteroides* ($P < 0.05$) were also notably elevated. In contrast, following HEP intervention, the abundances of *Lachnoclostridium*, *unclassified_Lachnospiraceae*, *Romboutsia*, *Blautia*, *Faecalibaculum*, and *Bacteroides* were markedly decreased ($P < 0.05$), whereas *Ileibacterium* ($P < 0.05$) were significant increased. These findings indicated that HEP effectively modulates the structural composition of the gut microbiota at the genus level in HFD-induced obese mice.

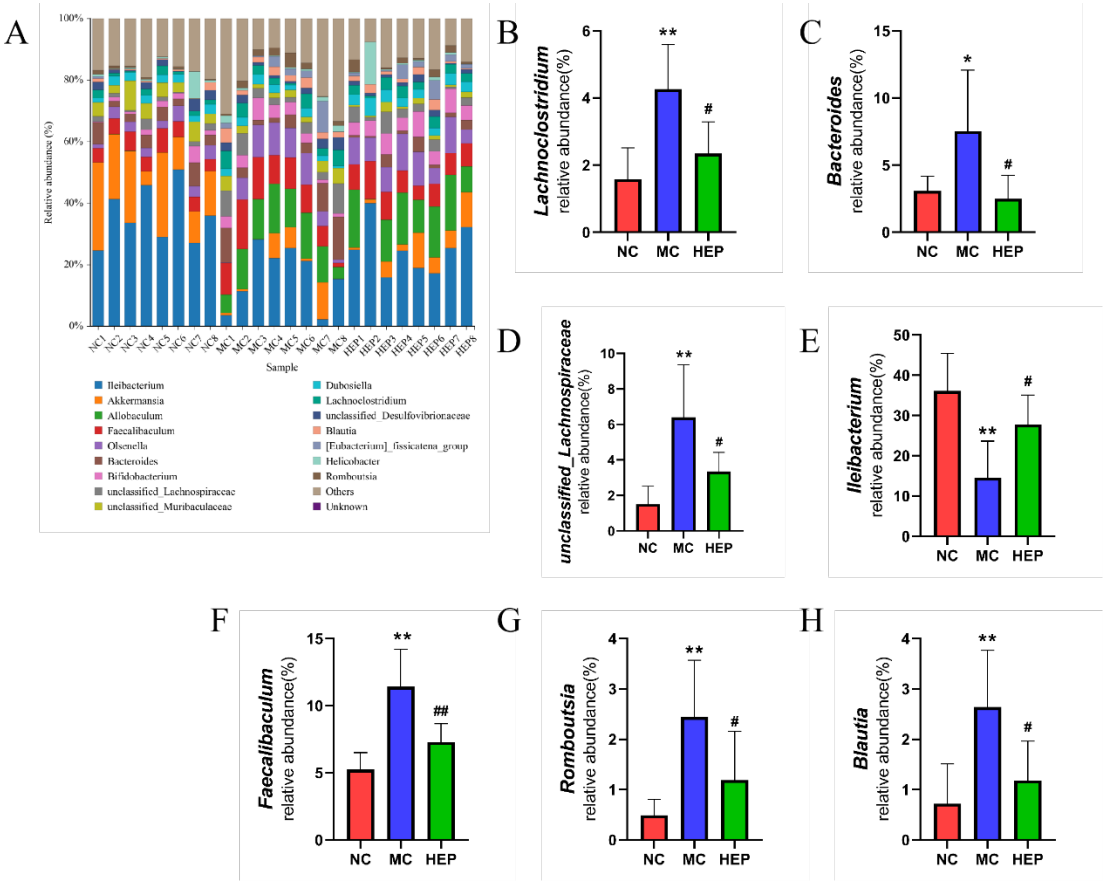



**Figure 11.** Genus-level microbial community analysis (A) Genus-level microbial community distribution; (B) *Lachnoclostridium*; (C) *Bacteroides*; (D) *unclassified_Lachnospiraceae*; (E) *Ileibacterium*; (F) *Faecalibaculum*; (G) *Romboutsia*; (H) *Blautia*

### *3.11.7 HEP Analysis of Differences Between Different Groups of Gut Microbiota*

As shown in the LDA value distribution histogram (Figure S4A), 12, 12, and 13 significantly different taxa were quantified in the NC, MC, and HEP groups. At the phylum level, Verrucomicrobiota in the NC group and Actinobacteriota in the HEP group could serve as potential biomarkers. Akkermansiaceae and Muribaculaceae in the NC group, Lachnospiraceae and Bacteroidaceae in the MC group, and Atopobiaceae and Bifidobacteriaceae in the HEP group were designated as biomarkers at the family level. *Ileibacterium*, *Akkermansia*, and *unclassified_Muribaculaceae* in the NC group, *Faecalibaculum*, *Bacteroides*, *unclassified_Lachnospiraceae*, and *Eubacterium_fissicatena_group* in the MC group, as well as *Allobaculum*, *Olsenella*, and *Bifidobacterium* in the HEP group, were considered characteristic genera at the genus level. *Ileibacterium valens*, *Akkermansia muciniphila*, *unclassified_Muribaculaceae*, and *Phocaeicola sartorii* in the NC group; *Faecalibaculum rodentium*, *Bacteroides vulgatus*, *unclassified_Lachnospiraceae*, and *Faecalicatena contorta* in the MC group; and *uncultured_Allobaculum sp.*, *Olsenella sp._oral_taxon_809*, and *Bifidobacterium pseudolongum* in the HEP group were designated as species-level biomarkers at the species level.

### *3.11.8 Predictive Analysis of HEP on Functional Genes of Intestinal Flora in Mice*

KEGG pathway prediction revealed that while the overarching microbial functional structure remained stable across groups (Figure 12A), specific shifts were induced by HFD and HEP (Figure 12C). Crucially,

HEP profoundly reshaped the microbial metabolic repertoire (Figure 12B), enriching "Glycan biosynthesis and metabolism" and "Lipid metabolism". The up-regulation of glycan metabolism provides bioinformatic evidence for an enhanced microbial capacity to ferment HEP structural carbohydrates. Concurrently, the enriched microbial lipid metabolism aligns robustly with the host's lipid-lowering phenotype and hepatic AMPK/SREBP-1c activation. Overall, these predictions suggested that HEP may reshape the metabolic potential of the gut microbiota, particularly pathways associated with carbohydrate utilization and lipid metabolism, which may contribute to improved metabolic homeostasis.

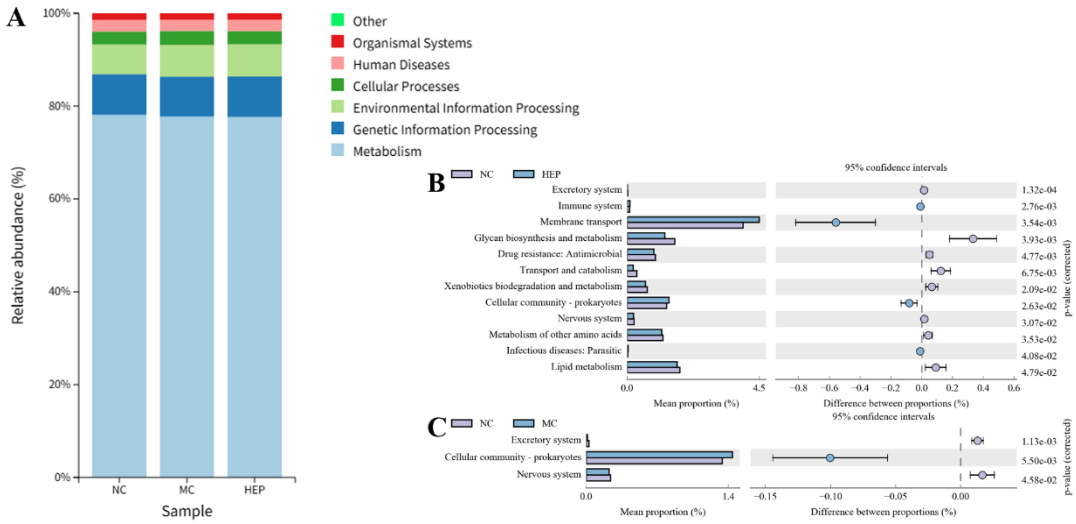



**Figure 12.** KEGG function prediction of gut microbiota (A) Histogram of functional composition; Relative abundance of predictive function genes between NC and HEP (B) NC and MC (C) in the first KEGG category.

### *3.11.9 Correlation Analysis of the Gut Microbiota with Other Indicators*

To highlight robust interactions, a Spearman's rank correlation network analysis was performed between the relative abundances of significantly altered microbial genera and host biochemical parameters (Figure 13). Beneficial taxa significantly enriched by HEP intervention, notably *Ileibacterium* and *Akkermansia*, exhibited strong positive correlations with intestinal barrier integrity markers (ZO-1 and occludin), SCFA concentrations (acetate, propionate, and butyrate), and the level of hepatic p-AMPK/AMPK ratio. Concurrently, these advantageous bacteria were significantly and negatively correlated with circulating atherogenic lipids, particularly TG and LDL-C. Conversely, obesity-associated genera that were heavily suppressed by HEP, including *Lachnoclostridium*, *Bacteroides*, *unclassified_Lachnospiraceae*, and *Blautia*, displayed an inverse pattern. These HFD-enriched taxa were significantly and positively associated with systemic lipid accumulation (TG, LDL-C), while exhibiting profound negative correlations with SCFA production, tight junction protein expressions, and hepatic p-AMPK/AMPK ratio. Collectively, these correlational networks supported a close association between gut microbial remodeling and improvements in host metabolic homeostasis.

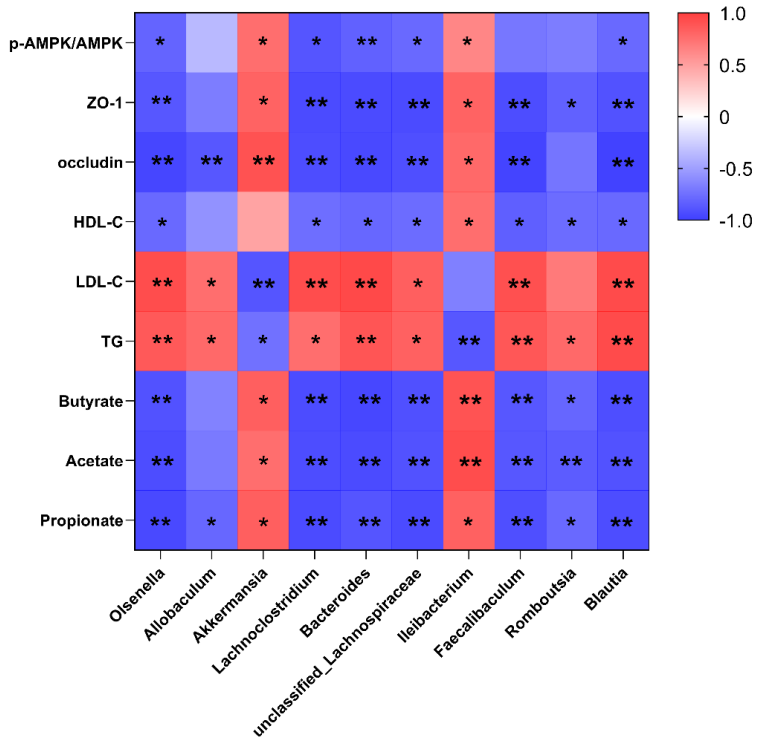



**Figure 13.** Spearman correlation analysis between gut microbiota and host metabolic parameters

### *3.12 The Effect of HEP on SCFAs in Mice*

By analyzing changes in SCFAs in feces, we further investigated HEP's inhibitory effect on obesity via the gut microbiota. Figure 14 demonstrated that the concentrations of individual SCFAs, including acetate, propionate, butyrate, and their branched-chain isomers, were markedly lower in the MC group relative to the NC group ($P < 0.01$). Relative to the MC group, following HEP gavage, fecal propionate, acetate and total SCFA concentrations were markedly elevated ($P < 0.01$) in mice. Isobutyrate and butyrate levels were also significantly increased ($P < 0.05$), while isovalerate and valerate levels showed non-significant upward trends. Taken together, these data demonstrated that HEP intake was associated with reversing the reduction in gut microbiota metabolites induced by HFD.

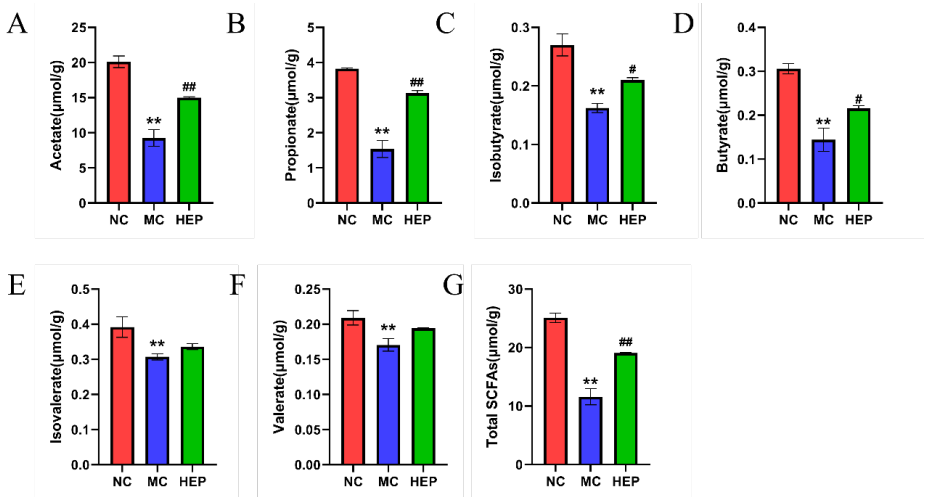



**Figure 14.** Levels of SCFAs in feces (A) Acetate; (B) Propionate; (C) Isobutyrate; (D) Butyrate; (E) Isovalerate; (F) Valerate; (G) Total SCFAs

## 4 Discussion

Obesity is a global public health crisis primarily characterized by dysregulated lipid metabolism, impaired insulin sensitivity, and concomitant metaflammation. The search for safe and effective natural bioactive compounds to intervene in obesity and its complications remains a critical research focus. The experimental results indicated that HEP significantly ameliorated excessive weight gain, alleviated lipid deposition, and restored both insulin sensitivity and glucose tolerance in HFD-fed mice. Concurrently, HEP modulated serum lipid profiles, attenuated the levels of systemic inflammatory cytokines, and exerted beneficial anti-obesity effects through multifaceted mechanisms. These mechanisms included modulation of hepatic AMPK/SREBP-1c-related lipid metabolism, restoration of intestinal barrier integrity, suppression of the TLR4/NF-κB inflammatory pathway, and remodeling of the intestinal microbiota architecture.

Analysis of growth indices, anatomical observations, and tissue histology revealed that HEP ameliorated HFD-induced epididymal adipocyte hypertrophy, reduced hepatic lipid droplet accumulation, and mitigated inflammatory manifestations. HFD typically leads to significant weight gain, substantial hepatic lipid deposition, and a marked expansion of epididymal and inguinal white adipose tissues [30, 31]. HEP intervention counteracted these effects, corroborating previous findings by Wang et al. [22], who reported that *Hericium erinaceus* reduced body fat accumulation in HFD mice. This suggested that HEP may alleviate lipid accumulation *in vivo*.

A core feature of metabolic dysfunction is compromised insulin sensitivity. Excessive intake of lipids and carbohydrates can trigger inflammatory responses and endoplasmic reticulum stress, which impede insulin signal transduction, ultimately leading to glucose and lipid metabolism disorders [32]. HEP effectively reversed the HFD-induced elevations in serum TG, LDL-C and T-CHO levels while increasing HDL-C levels. INS and LEP, which are crucial for regulating blood glucose levels, increasing energy expenditure, and reducing fat storage [33], were also significantly normalized. Furthermore, HEP significantly reduced the AUCs for both the OGTT and ITT, indicating the effective improvement of HFD-induced disturbances of carbohydrate metabolism, thereby partly recovering glucoregulatory function. Cui et al. [24] found that HEP improved glucose metabolism imbalance by activating the IRS/PI3K pathway and promoting hepatic glycogenesis. Therefore, whether HEP also engages the IRS/PI3K axis warrants further investigation.

Consistent with its lipid-lowering efficacy in the serum (characterized by reduced LDL-C, T-CHO and TG levels, and elevated HDL-C), HEP also exerted profound protective effects against hepatic lipid accumulation. AMPK coordinates multiple metabolic pathways to restore energy balance, including suppressing lipid synthesis while enhancing fatty acid oxidation. AMPK regulates lipid metabolism by influencing several downstream targets, with SREBP-1c being one of its key targets [34, 35]. Our results revealed that HEP intervention significantly increased the p-AMPK/AMPK ratio. Simultaneously, HEP significantly suppressed the expression of SREBP-1c and its downstream targets FAS and ACC. This concomitant activation of AMPK and suppression of the SREBP-1c lipogenic network indicated that HEP may contribute to the improvement of hepatic lipid metabolism [24]. These molecular alterations were

accompanied by reduced expression of lipogenic proteins, which was consistent with the alleviation of hepatic steatosis observed in HFD-fed mice.

A pivotal factor underlying obesity-induced metabolic pathologies is the persistence of subclinical chronic inflammation [36], while obesity itself can enhance intestinal permeability [12], allowing harmful substances into the bloodstream and driving further systemic chronic inflammation [37, 38]. Histopathological results indicated that HEP significantly ameliorated HFD-induced colonic tissue edema, crypt structure destruction, and goblet cell reduction. The reinforcement of gut barrier integrity by HEP was associated with the enhanced synthesis of tight junction proteins at both mRNA and protein levels, a mechanism that supports the findings documented by Tian et al [21]. Restoration of barrier function further restricts the systemic translocation of inflammatory signals such as LPS. HEP significantly inhibited the TLR4 level and the phosphorylation levels of IKKα/β and NF-κB p65 in colon, concomitantly reducing serum levels of IL-6, IL-1β and TNF-α. The TLR4/NF-κB pathway was a major driver of intestinal inflammation, and LPS can trigger the TLR4/NF-κB pathway [39]. Therefore, we inferred that HEP alleviated obesity-associated inflammation via the axis of "repairing intestinal barrier- blocking endotoxin translocation - inhibiting the TLR4/NF-κB pathway." Mishra et al. indicated that the intestinal flora in HFD individuals reduced ZO-1 expression, thereby weakening intestinal barrier function and exacerbating inflammation [40]. Consequently, we hypothesized that HEP's restoration of intestinal barrier function and amelioration of inflammation may be achieved via modulation of the gut microbiota, warranting further investigation into the effects of HEP on microbial communities.

The intestinal microbiome has emerged as a vital driver in the pathogenesis of obesity [41]. Possessing the capacity to induce fat accumulation in the host, the gut microbiota significantly influenced the development of HFD obesity and holds potential pathogenic roles in human obesity [42]. The multifaceted anti-obesity effects of HEP are underpinned by its capacity to reshape the gut microecology and fortify the intestinal-hepatic axis. Experimental results indicated that HEP may achieve anti-obesity effects via regulating intestinal microbiota composition. Within the intestinal flora, Firmicutes and Bacteroidota were closely associated with metabolic disorders. Several studies have linked an increased F/B ratio to obesity and intestinal inflammation [43]. In particular, Turnbaugh et al. illustrated that obese mice exhibited an elevated ratio of F/B compared to lean mice [44], a pattern that was consistently observed in our study. Following HEP intervention, this ratio decreased, confirming HEP's anti-obesity efficacy. Existing literature indicated that Firmicutes harbor carbohydrate metabolism enzymes that influence energy absorption [45], while Bacteroidota suppressed gut inflammation and enhanced tight junctions by dampening NF-κB activation [46]. HEP also markedly increased the abundance of Verrucomicrobiota, a phylum represented primarily by *Akkermansia*. *Akkermansia* has been widely recognized for its ability to degrade mucin while simultaneously stimulating mucus turnover, thereby reinforcing the intestinal mucus layer and enhancing epithelial barrier integrity [13, 25, 47]. Therefore, it is hypothesized that HEP may exert its anti-obesity effects at phylum level by altering the F/B ratio and regulating the abundance of Verrucomicrobiota, thereby influencing energy absorption, alleviating

inflammatory responses, and reinforcement of gut barrier homeostasis. At the genus level, existing literature indicates that *Ileibacterium* exhibites anti-obesity effects [48], while *Faecalibacterium* and *Romboutsia* have been reported to be positively correlated with obesity levels [49]. HEP markedly elevated the abundance of beneficial gut microbes ($P < 0.05$), such as *Ileibacterium*, while notably reducing the abundance of harmful gut microbes associated with obesity, such as *Romboutsia* and *Lachnoclostridium*. In addition to taxonomic alterations, the predictive functional analysis further suggested that HEP reshaped the metabolic potential of the gut microbiota. Specifically, the enrichment of glycan biosynthesis and metabolism suggested an enhanced microbial capacity to utilize HEP-derived carbohydrates as fermentable substrates, whereas the enrichment of lipid metabolism-related pathways is in agreement with the improved serum lipid profile and reduced hepatic lipid accumulation observed in HEP-treated mice. Although KEGG analysis based on 16S rRNA sequencing provides only predictive functional information rather than direct metagenomic evidence, the observed enrichment of carbohydrate- and lipid metabolism-related pathways was consistent with the improved metabolic phenotype and increased SCFA levels observed in HEP-treated mice. Correlation analysis further strengthened the potential linkage between gut microbiota remodeling and host metabolic improvement. These findings suggested that alterations in microbial composition were closely associated with improvements in intestinal barrier integrity, microbial metabolite production, and host lipid metabolism.

SCFAs are known to promote tight junction integrity and key aspects of host metabolism [39]. Notably, the enrichment of these SCFA-producing bacteria, especially those producing butyrate, was positively correlated with the up-regulation of tight junction proteins, suggesting a potential association between microbial metabolite production and intestinal barrier maintenance [50]. This structural reinforcement may contribute to reduced LPS translocation and attenuated TLR4/NF-κB inflammatory signaling. Furthermore, the mitigation of systemic metaflammation and the altered metabolic flux of microbial-derived SCFAs may be associated with altered phosphorylation of hepatic AMPK. These observations raised the possibility that SCFA-mediated metabolic signaling may participate in the modulation of AMPK/SREBP-1c signaling, thereby contributing to improved lipid metabolism [11, 51, 52]. Interestingly, the results of the correlation analysis showed that the level of p-AMPK/AMPK in the liver was positively correlated with the production of SCFAs and the barrier-fortifying bacteria, while negatively correlated with the bacteria associated with obesity [53]. Although these statistical associations did not establish causality, they support the possibility that gut microbiota-derived metabolites may participate in the regulation of hepatic energy metabolism through the microbiota–gut–liver axis. Collectively, the taxonomic, functional prediction, and correlation analyses consistently indicated that HEP not only remodeled the composition of the gut microbiota but also altered its metabolic potential and strengthened the association between microbial communities and host metabolic homeostasis. These findings further supported the involvement of the microbiota–gut–liver axis in the anti-obesity effects of HEP.

In summary, HFD disrupted the architecture and abundance of the gut microbiota, increased intestinal permeability, and subsequently triggered systemic metaflammation and glucolipid metabolic disorders.

Meanwhile, HEP intake exhibited beneficial effects in alleviating obesity and inflammation through a multi-target mechanism, including modulating the gut microbiota, repairing the intestinal barrier, and improving glucose and lipid metabolism. This study provided a comprehensive new perspective on the ability of HEP to reshape the gut microbiota and mitigate obesity. However, this work has limitations. First, based on body surface area conversion, the administered dose of HEP (200 mg/kg/day in mice) corresponds to approximately 1.13 g/day for a 70-kg adult. Although this dosage is considered physiologically achievable in the form of concentrated polysaccharide-based functional foods or dietary supplements, the implementation of a single-dose regimen still restricted the evaluation of dose-response relationships and the identification of the minimum effective or optimal intervention dosage. Second, although Spearman correlation analysis revealed significant associations between gut microbiota remodeling, SCFA production, and improved metabolic parameters, correlation does not imply causation. The current study lacks definitive loss-of-function experiments, such as fecal microbiota transplantation or antibiotic depletion models, which prevent us from firmly establishing a causal role for the gut microbiota. Additionally, while the present study demonstrated a clear correlation between HEP administration and increased hepatic p-AMPK expression, the definitive requirement of AMPK activation for the anti-obesity efficacy of HEP remains to be fully established using specific AMPK agonists, antagonists, or gene knockout models. Future investigations should include dose-response experiments to determine the minimum effective dose, optimal intervention dose, and long-term safety. Furthermore, pharmacological or genetic blockers should be incorporated to conclusively determine the indispensability of AMPK signaling in HEP-mediated metabolic recovery.

## 5 Conclusion

In this research, a HFD mouse model was established and the hypoglycemic and hypolipidemic effects of HEP on obese mice were investigated through experiments including body weight monitoring, histomorphological examination of organs, analysis of serum lipid and inflammatory factors, intestinal permeability assessment, and gut microbiota analysis. Results indicated that HEP ameliorated HFD-induced obesity, which was accompanied by improved intestinal barrier function, modulation of inflammatory responses, and remodeling of gut microbiota. These findings suggested its potential application for functional food development.

## Conflicts of interest

The authors declare that they have no known competing financial interests or personal relationships that could have appeared to influence the work reported in this paper.

## Acknowledgments

This work was sponsored by the Zhejiang Provincial Key Research and Development Program (2025C04030 & 2022C04036 & 2023C02040), the professional development program for domestic visiting scholars in the universities of the education department of Zhejiang Province in 2025, Sichuan Provincial Key Research and Development Program (2024YFHZ0179), Industry-University Cooperation Project Fund of

Zhejiang University of Technology (KYY-HX-20211132 & KYY-HX-202402440), and Shaoxing City Science and Technology Special Project to Strengthen Agriculture (2024A12002) and National College Student Innovation and Entrepreneurship Training Program (X2025103370004).

## Availability of data and material

The data that support the findings of this study are available on request from the corresponding author upon reasonable request.

## References

[1] F. Emanuela, M. Grazia, D.R. Marco, et al., Inflammation as a link between obesity and metabolic syndrome, Journal of nutrition. 2012 (2012) 476380.

[2] J. Liu, Z. He, N. Ma, et al., Beneficial effects of dietary polyphenols on high-fat diet-induced obesity linking with modulation of gut microbiota, Journal of Agricultural Food Chemistry. 68 (2019) 33-47.

[3] T.-R. Wu, C.-S. Lin, C.-J. Chang, et al., Gut commensal *Parabacteroides goldsteinii* plays a predominant role in the anti-obesity effects of polysaccharides isolated from *Hirsutella sinensis* Gut. 68 (2019) 248-262. https://doi.org/10.1136/gutjnl-2017-315458.

[4] L.R. Howe, K. Subbaramaiah, C.A. Hudis, et al., Molecular pathways: adipose inflammation as a mediator of obesity-associated cancer, Clinical cancer research 19 (2013) 6074-6083.

[5] H.E. Bays, P.H. Jones, T.A. Jacobson, et al., Lipids and bariatric procedures part 1 of 2: scientific statement from the National Lipid Association, American Society for Metabolic and Bariatric Surgery, and obesity medicine association: FULL REPORT, Journal of clinical lipidology. 10 (2016) 33-57.

[6] J. Geng, Q. Ni, W. Sun, et al., The links between gut microbiota and obesity and obesity related diseases, Biomedicine & Pharmacotherapy. 147 (2022) 112678. https://doi.org/10.1016/j.biopha.2022.112678.

[7] H. Yanai, H. Yoshida, Beneficial Effects of Adiponectin on Glucose and Lipid Metabolism and Atherosclerotic Progression: Mechanisms and Perspectives, International Journal of Molecular Sciences. 20 (2019) 1190. 1190. https://doi.org/10.3390/ijms20051190.

[8] B.K. Perler, E.S. Friedman, G.D. Wu, The Role of the Gut Microbiota in the Relationship Between Diet and Human Health, Annual Review of Physiology. 85 (2023) 449-468. https://doi.org/10.1146/annurev-physiol-031522-092054.

[9] A.C. Gomes, C. Hoffmann, J.F. Mota, The human gut microbiota: Metabolism and perspective in obesity, Gut microbes. 9 (2018) 308-325.

[10] I.J. Malesza, M. Malesza, J. Walkowiak, et al., High-Fat, Western-Style Diet, Systemic Inflammation, and Gut Microbiota: A Narrative Review, Cells. 10 (2021) 3164. https://doi.org/10.3390/cells10113164.

[11] N. Wang, Y. Dilixiati, L. Xiao, et al., Different Short-Chain Fatty Acids Unequally Modulate Intestinal Homeostasis and Reverse Obesity-Related Symptoms in Lead-Exposed High-Fat Diet Mice, Journal of Agricultural and Food Chemistry. 72 (2024) 18971-18985. https://doi.org/10.1021/acs.jafc.4c04193.

[12] M.W. Rohr, C.A. Narasimhulu, T.A. Rudeski-Rohr, et al., Negative Effects of a High-Fat Diet on Intestinal Permeability: A Review, Advances in Nutrition. 11 (2020) 77-91. https://doi.org/10.1093/advances/nmz061.

[13] J. Ye, Y. Jiang, K. Yang, et al., Changyanning Ameliorates Dextran Sodium Sulfate-Induced Colitis by Modulating Gut Microbiota Inflammation and Intestinal Barrier in Mice, Molecular Nutrition & Food Research. (2026) https://doi.org/10.1002/mnfr.70461.

[14] L.K. Stenman, R. Holma, R. Korpela, High-fat-induced intestinal permeability dysfunction associated with altered fecal bile acids, World journal of gastroenterology: WJG. 18 (2012) 923.

[15] O.E. Panel, A.C.o. Cardiology, A.H.A.T.F.o.P. Guidelines, Expert Panel Report: Guidelines (2013) for the management of overweight and obesity in adults, Obesity. 22 (2014) S41-S410.

[16] D.M. Steinberg, D.F. Tate, G.G. Bennett, et al., The efficacy of a daily self-weighing weight loss intervention using smart scales and e-mail, Obesity. 21 (2013) 1789-1797.

[17] S.B. Heymsfield, T.A. Wadden, Mechanisms, pathophysiology, and management of obesity, New England Journal of Medicine. 376 (2017) 254-266.

[18] Y. Yu, M. Shen, Q. Song, et al., Biological activities and pharmaceutical applications of polysaccharide from natural resources: A review, Carbohydrate polymers. 183 (2018) 91-101.

[19] S. Li, J. Yi, X. Yu, et al., Preparation and characterization of pullulan derivative/chitosan composite film for potential antimicrobial applications, International Journal of Biological Macromolecules. 148 (2020) 258-264.

[20] H. Xue, P. Zhang, C. Zhang, et al., Research progress in the preparation, structural characterization, and biological activities of polysaccharides from traditional Chinese medicine, International Journal of Biological Macromolecules. 262 (2024) 129923.

[21] B. Tian, P. Wang, T. Xu, et al., Ameliorating effects of *Hericium erinaceus* polysaccharides on intestinal barrier injury in immunocompromised mice induced by cyclophosphamide, Food & Function. (2023) https://doi.org/10.1039/d2fo03769f.

[22] G.Z. Wang, B.B. Wang, Q. Zhou, et al., Puerarin combined with *Hericium erinaceus* insoluble dietary fiber alleviates obesity induced by high-fat diet through regulating the glycerophospholipid metabolism pathway influenced by gut microbiota, Applied and Environmental Microbiology. 91 (2025) https://doi.org/10.1128/aem.02376-24.

[23] B. Tian, Y. Geng, T. Xu, et al., Digestive Characteristics of *Hericium erinaceus* Polysaccharides and Their Positive Effects on Fecal Microbiota of Male and Female Volunteers During in vitro Fermentation, Frontiers in Nutrition. (2022) https://doi.org/10.3389/fnut.2022.858585.

[24] W. Cui, X. Song, X. Li, et al., Structural characterization of *Hericium erinaceus* polysaccharides and the mechanism of anti-T2DM by modulating the gut microbiota and metabolites, International Journal of Biological Macromolecules. 242 (2023) 125165. https://doi.org/https://doi.org/10.1016/j.ijbiomac.2023.125165.

[25] B. Tian, Y. Pan, X. Zhang, et al., Etiolated-green tea attenuates colonic barrier dysfunction and inflammation in high-fat diet-induced mice by modulating gut microbiota, Food research international. 197 (2024) 115192. https://doi.org/10.1016/j.foodres.2024.115192.

[26] A. Yoo, M. Jung Kim, J. Ahn, et al., Fuzhuan brick tea extract prevents diet-induced obesity via stimulation of fat browning in mice, Food chemistry. 377 (2022) 132006. https://doi.org/10.1016/j.foodchem.2021.132006.

[27] B. Tian, R. Liu, T. Xu, et al., Modulating effects of *Hericium erinaceus* polysaccharides on the immune response by regulating gut microbiota in cyclophosphamide-treated mice, J. Sci. Food Agric. 103 (2023) 3050.

[28] P. Wang, M. Cai, K. Yang, et al., Phenolics from Dendrobium officinale Leaf Ameliorate Dextran Sulfate Sodium-Induced Chronic Colitis by Regulating Gut Microbiota and Intestinal Barrier, Journal of Agricultural and Food Chemistry. 71 (2023) 16630-16646. https://doi.org/10.1021/acs.jafc.3c05339.

[29] X.-Y. Wang, J.-Y. Yin, S.-P. Nie, et al., Isolation, purification and physicochemical properties of polysaccharide from fruiting body of *Hericium erinaceus* and its effect on colonic health of mice, International Journal of Biological Macromolecules. 107 (2018) 1310-1319. https://doi.org/https://doi.org/10.1016/j.ijbiomac.2017.09.112.

[30] H. Cai, J. Zhang, C. Liu, et al., High-fat diet-induced decreased circulating bile acids contribute to obesity associated with gut microbiota in mice, Foods. 13 (2024) 699.

[31] J.J. Tan, R.Z. Hu, J.T. Gong, et al., Protection against Metabolic Associated Fatty Liver Disease by Protocatechuic Acid, Gut Microbes. 15 (2023) 2238959. https://doi.org/10.1080/19490976.2023.2238959.

[32] S. Xu, J. Xi, T. Wu, et al., The role of adipocyte endoplasmic reticulum stress in obese adipose tissue dysfunction: a review, International Journal of General Medicine. (2023) 4405-4418.

[33] U. Ezeh, Z. Arzumanyan, D. Lizneva, et al., Alterations in plasma non-esterified fatty acid (NEFA) kinetics and relationship with insulin resistance in polycystic ovary syndrome, Human Reproduction. 34 (2019) 335-344.

[34] Z. Meng, Q. Liu, F. Sun, et al., Hepatitis C virus nonstructural protein 5A perturbs lipid metabolism by modulating AMPK/SREBP-1c signaling, Lipids in health and disease. 18 (2019) 191. https://doi.org/10.1186/s12944-019-1136-y.

[35] T. Lan, X.-j. Geng, S.-j. Zhang, et al., Si-Ni-San inhibits hepatic Fasn expression and lipid accumulation in MAFLD mice through AMPK/p300/SREBP-1c axis, Phytomedicine. (2024),

[36] T.P. Scheithauer, E. Rampanelli, M. Nieuwdorp, et al., Gut microbiota as a trigger for metabolic inflammation in obesity and type 2 diabetes, Frontiers in immunology. 11 (2020) 571731.

[37] Y. Wu, J. Li, W. Ding, et al., Enhanced intestinal barriers by puerarin in combination with tryptophan, Journal of Agricultural Food Chemistry. 69 (2021) 15575-15584.

[38] J. Huo, Z. Wu, W. Sun, et al., Protective effects of natural polysaccharides on intestinal barrier injury: A review, Journal of agricultural food chemistry. 70 (2022) 711-735.

[39] B. Tian, P. Huang, Y. Pan, et al., Tea Polyphenols Reduced Obesity by Modulating Gut Microbiota-SCFAs-Barrier and Inflammation in High-Fat Diet-Induced Mice, Molecular Nutrition & Food Research. 68 (2024) 2400685. https://doi.org/https://doi.org/10.1002/mnfr.202400685.

[40] S.P. Mishra, B. Wang, S. Jain, et al., A mechanism by which gut microbiota elevates permeability and inflammation in obese/diabetic mice and human gut, Gut. 72 (2023) 1848-1865.

[41] L. Sun, L. Ma, Y. Ma, et al., Insights into the role of gut microbiota in obesity: pathogenesis, mechanisms, and therapeutic perspectives, Protein cell. 9 (2018) 397-403.

[42] L. Zhao, The gut microbiota and obesity: from correlation to causality, Nature Reviews Microbiology. 11 (2013) 639-647. https://doi.org/10.1038/nrmicro3089.

[43] J. Schachter, J. Martel, C.-S. Lin, et al., Effects of obesity on depression: a role for inflammation and the gut microbiota, Brain, behavior, immunity. 69 (2018) 1-8.

[44] P.J. Turnbaugh, R.E. Ley, M.A. Mahowald, et al., An obesity-associated gut microbiome with increased capacity for energy harvest, nature. 444 (2006) 1027-1031.

[45] P. Liu, W. Zhou, W. Xu, et al., The main anthocyanin monomer from Lycium ruthenicum Murray fruit mediates obesity via modulating the gut microbiota and improving the intestinal barrier, Foods. 11 (2021) 98.

[46] Y. Wu, X. Zhang, X. Liu, et al., Galactooligosaccharides and Limosilactobacillus reuteri synergistically alleviate gut inflammation and barrier dysfunction by enriching Bacteroides acidifaciens for pentadecanoic acid biosynthesis, Nature Communications. 15 (2024) 9291.

[47] B. Tian, J. Zhao, M. Zhang, et al., Lycium ruthenicum Anthocyanins Attenuate High-Fat Diet-Induced Colonic Barrier Dysfunction and Inflammation in Mice by Modulating the Gut Microbiota, Molecular Nutrition & Food Research. 65 (2021) 2000745. https://doi.org/https://doi.org/10.1002/mnfr.202000745.

[48] Y. Meng, Q. Meng, C. Li, et al., A comparison between partially peeled hulless barley and whole grain hulless barley: beneficial effects on the regulation of serum glucose and the gut microbiota in high-fat diet-induced obese mice, Food Function. 14 (2023) 886-898.

[49] Y. Luo, Y. Wen, J. Huang, et al., Matcha alleviates obesity by modulating gut microbiota and its metabolites, Current Research in Food Science. 9 (2024) 100823.

[50] P. Huang, J. Hu, K. Yang, et al., Digestion characteristics of Changyanning formula and its regulatory effect on fecal microbiota and metabolites during in vitro fermentation, Fitoterapia. 187 (2025) 106949. https://doi.org/https://doi.org/10.1016/j.fitote.2025.106949.

[51] H. Li, S. Liu, H. Chen, et al., Gut dysbiosis contributes to SCFAs reduction-associated adipose tissue macrophage polarization in gestational diabetes mellitus, Life Sciences. 350 (2024) 122744. https://doi.org/https://doi.org/10.1016/j.lfs.2024.122744.

[52] Y. Ren, Q. Sun, R. Gao, et al., Low Weight Polysaccharide of *Hericium erinaceus* Ameliorates Colitis via Inhibiting the NLRP3 Inflammasome Activation in Association with Gut Microbiota Modulation, Nutrients. 15 (2023) 739. https://doi.org/10.3390/nu15030739.

[53] B. Tian, Y. Pan, X. Zhou, et al., Yellow leaf green tea modulates the AMPK/ACC/SREBP1c signaling pathway and gut microbiota in high-fat diet-induced mice to alleviate obesity, Journal of the Science of Food and Agriculture. (2024) https://doi.org/10.1002/jsfa.13413.